

## Direct-reaction model for $(p, \gamma)$ reactions to highly excited states in $^{12}\text{C}$

J. T. Londergan and L. D. Ludeking

*Department of Physics, Indiana University, Bloomington, Indiana 47405*

(Received 13 May 1981)

Proton radiative capture reactions on  $^{11}\text{B}$  targets are calculated assuming a direct capture mechanism. This is used to predict  $(p, \gamma)$  transitions leading to the ground state of  $^{12}\text{C}$ , and to high-lying excited states at about 19 MeV excitation in  $^{12}\text{C}$ . The results are compared with recent experimental data. The theoretical cross sections are the same magnitude as the data, but do not properly reproduce the energy dependence of the capture cross sections. There appears to be an important "semidirect" component to the  $(p, \gamma)$  reaction leading to high-lying states in  $^{12}\text{C}$ . We have also applied the same theory to calculate  $^{12}\text{C}(\gamma, p_0)^{11}\text{B}$  and  $^{12}\text{C}(\gamma, n_0)^{11}\text{C}$  transitions which have been previously measured.

[NUCLEAR REACTIONS  $(p, \gamma)$  and  $(\gamma, p)$  reactions at medium energies;  
direct capture; states of high excitation energy in  $^{12}\text{C}$ ; photodisintegration of  $^{12}\text{C}$ .]

### I. INTRODUCTION

Proton radiative capture measurements (or the time-reversed photodisintegration cross sections) have been very useful both in reaction mechanism studies and in elucidating aspects of nuclear structure. Historically, low energy measurements (up to about 30 MeV proton energy) have been studied in detail in both experiment and theory. Measurement of  $\sigma(\theta)$  and nucleon analyzing power leads to a rather complete knowledge of capture amplitudes and can be used to map out strength functions in low-energy nucleon-nucleus scattering. Recent reviews of this area are given in Refs. 1–4. The role of giant multipole resonances (GDR) built on the ground state of a nuclear target is relatively well understood.<sup>4</sup> The original direct-capture calculations of Lane and Lynn<sup>5</sup> failed to reproduce experimental data in the GDR region. The theoretical basis for this process was first provided by Brown,<sup>6</sup> Clement, Lane, and Rook,<sup>7</sup> and Lushnikov and Zaretsky,<sup>8</sup> and this picture has been supported by numerous continuum coupled-channel models of these reactions.<sup>9–14</sup> Several groups have used doorway-state models<sup>15–17</sup> to describe these reactions. In many cases, a detailed understanding of the structure in this energy region has required extensive experimental effort—this is particularly true in  $^{12}\text{C}$ , which we

discuss in this paper<sup>16,18,19</sup>—where we now have a fairly complete set of data regarding the ground state transitions  $(p, \gamma_0)$ .

At higher energies the situation is less clear due to the paucity of experimental data.<sup>20–32</sup> Considerable theoretical effort is presently devoted to investigating the relative importance of direct-reaction processes and exchange-current terms at these energies.<sup>33–38</sup> Although this question is not yet resolved, it is clear that any satisfactory theory of the  $(\gamma, p)$  reaction must simultaneously be able to explain the existing  $(\gamma, n_0)$  data.

An extensive set of proton radiative capture experiments has been carried out on several nuclei at the Indiana University Cyclotron Facility (IUCF), for proton energies 25–80 MeV.<sup>39–42</sup> These data provide cross sections as well as asymmetries, for radiative capture to the ground state and discrete low-lying states of the residual nucleus. One of the most striking features of the data was the observation that a great deal of the total capture strength in these reactions was concentrated in  $(p, \gamma)$  transitions to a relatively highly-excited state, or groups of states, in the residual nucleus.

This is illustrated in Fig. 1, which shows the photon spectrum from the  $(p, \gamma)$  reaction on  $^{11}\text{B}$  at a photon angle of  $60^\circ$  relative to the incident proton ( $E_{\text{lab}} = 23.7$  MeV).<sup>41</sup> The higher  $\gamma$  energies

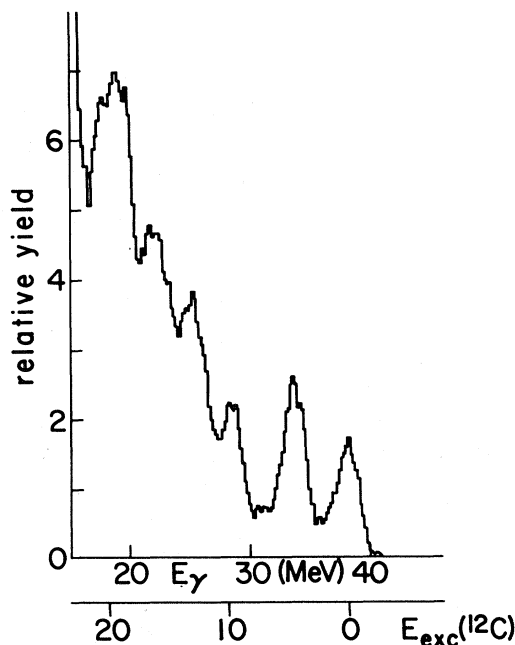


FIG. 1. The spectrum of photons from the  $^{11}\text{B}(p,\gamma)$  reaction measured at IUCF by Blatt *et al.*, Refs. 41 and 42. Photon energy vs photon cross section  $d^2\sigma/d\Omega dE_\gamma$ , in arbitrary units, resulting from  $E_p=23.7$  MeV at a photon angle  $\theta_\gamma$  of  $60^\circ$ . Also shown is the excitation energy in the  $A=12$  system corresponding to each photon energy.

correspond to lower excitation energy in the residual  $A=12$  nucleus. Distinct peaks can be seen leading to the ground state and first excited states in  $^{12}\text{C}$ . A prominent feature of this excitation spectrum is the large photon yield to a state or states in the  $A=12$  system corresponding to excitation energy of about 19 MeV relative to the  $^{12}\text{C}$  ground state. Although these energies are above particle emission threshold, in a simple shell model particle-hole approach the  $(1d_{5/2}^5)$  single-particle strength is expected to be concentrated in this region.

In Fig. 2, we show a  $^{12}\text{C}(p,\gamma)$  photon spectrum, also at  $60^\circ$ , for  $E_{\text{lab}}=28.5$  MeV. Again, the photon spectrum leading to the  $^{13}\text{N}$  ground state and first excited state are visible. In this case there is a strong peak leading to states in the vicinity of the  $J^\pi=(\frac{3}{2}^+)$  state of  $^{13}\text{N}$  at 3.6 MeV excitation energy. These  $(p,\gamma)$  data provide the radiative capture transitions to discrete low-lying states in the residual nucleus, however, they also show that the bulk of the capture strength is going to a concentrated group of particle-unbound states in the residual nucleus. This raises the question of whether such strong transitions may be understood as a direct

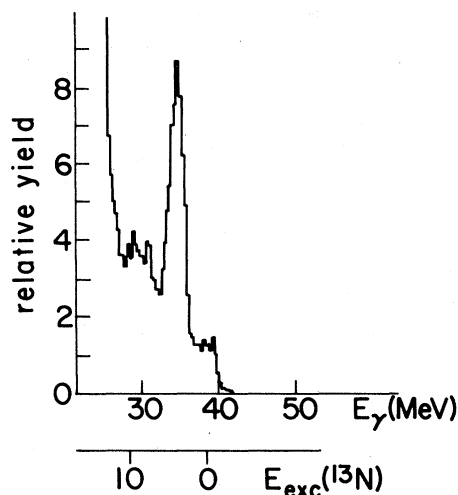


FIG. 2. The spectrum of photons resulting from the  $^{12}\text{C}(p,\gamma)$  reaction.  $E_p=28.5$  MeV and  $\theta_\gamma=60^\circ$ . Photon energy vs photon cross section  $d^2\sigma/d\Omega dE_\gamma$  in arbitrary units.

capture process, or if more complicated structure or reaction mechanism effects are necessary to explain these data.

We present calculations which represent an attempt to analyze the  $(p,\gamma)$  reaction leading to excited nuclear states by a direct reaction mechanism. An earlier calculation by Tsai and Londergan<sup>43</sup> (hereafter referred to as TL) investigated the contribution to these reactions using an effective interaction plus a residual interaction. In that model, the major contribution to the cross sections came from the two-body currents mediated by the residual interaction. The proton-nucleus interaction was written as the sum of a shell-model one-body potential and a residual two-particle interaction. The "shell-model" potential used was a Woods-Saxon potential whose strength had been adjusted by Birkholz<sup>11</sup> to reproduce the binding energy of the  $1s$  and  $1p$  single-particle wave functions. This potential is much stronger than conventional optical potentials and has no absorption. Fink *et al.*<sup>44</sup> have shown that photodisintegration reactions are very sensitive to the strength of the proton-nucleus interaction, and that the calculated  $(\gamma,p_0)$  cross section tends to increase as the strength of the nucleon-nucleus interaction decreases.

In this paper we examine whether the direct-reaction spectator model for the  $(p,\gamma)$  reactions can correctly predict the observed  $(p,\gamma)$  behavior, particularly the transitions to states at 19 MeV in  $^{12}\text{C}$ . We assume that the incident proton radiates a photon and makes a transition from the incident con-

tinuum state to a (bound or unbound) single-particle final state relative to the initial target nucleus. For the nuclear current operator, the proton convection current and spin magnetization current are used. An optical potential is used to describe the nuclear interaction of the incident proton and target. Finally, we calculate the final nucleon shell-model state using a single-particle potential which has been used to treat  $(p, \gamma)$  reactions on  $^{12}\text{C}$  in the vicinity of the giant dipole resonance.

Section II describes the theoretical formulation of this model. In Sec. III we present our results and discuss the application to the reactions  $^{11}\text{B}(p, \gamma_0)^{12}\text{C}$  and  $^{11}\text{B}(p, \gamma_{19})^{12}\text{C}^*$  (by this we mean transitions leading to the observed final state leaving the residual  $^{12}\text{C}$  nucleus at an excitation energy between 18.4–20.6 MeV). We also extend our calculations upward in energy to analyze the existing  $^{12}\text{C}(\gamma, p_0)^{11}\text{B}$  and  $^{12}\text{C}(\gamma, n_0)^{11}\text{C}$  data. In Sec. IV we review our results and present our conclusions.

## II. RADIATIVE CAPTURE IN A DIRECT-CAPTURE SPECTATOR MODEL

For nucleon radiative capture reactions, we must evaluate the transition amplitude

$$M_{fi}^{(\lambda)} = - \int d\vec{r} \langle \psi_f | \vec{j}(\vec{r}) \cdot \vec{A}_\lambda(\vec{r}) | \psi_i \rangle. \quad (2.1)$$

In Eq. (2.1),  $\psi_i$  is the nuclear wave function, which is composed of an incident proton of momentum  $k_i$  and the ground state of the target nucleus.  $\vec{A}_\lambda(\vec{r})$  is the electromagnetic potential for creation of a photon with momentum  $\vec{k}_\gamma$  and helicity  $\lambda$ , and has the form

$$\vec{A}_\lambda(\vec{r}) = \frac{2\pi}{\omega_\gamma} \vec{\epsilon}_\gamma^*(\vec{k}_\gamma) e^{-i\vec{k}_\gamma \cdot \vec{r}}. \quad (2.2)$$

Here,  $\omega_\gamma = |\vec{k}_\gamma|$  is the photon energy, and  $\vec{\epsilon}_\gamma(\vec{k}_\gamma)$  is the photon polarization vector of helicity  $\lambda$ . All equations are presented in the radiation gauge and we use units in which  $\hbar = c = 1$ . The final state of the nuclear system is denoted by  $\psi_f$ .

We calculate the transition amplitudes in a spectator formalism; that is, the incident nucleon is assumed to radiate a photon in the presence of the strong field of the target, and the final state of the system can be factorized into the product of a wave function for the target nucleus in its original state and the incident nucleon in a single-particle (shell model) state relative to the target. The direct-reaction model for the  $(p, \gamma)$  process neglects the coupling of excited target states in the radiative

capture reaction.

This model is shown graphically in Fig. 3. The incident nucleon of momentum  $\vec{k}_i$  is distorted in the field of the target nucleus, which is initially in state  $A_i$ . The nucleon radiates a photon of momentum  $\vec{k}_\gamma$  and makes a transition to the single particle state  $f$  relative to the target. The “spectator” approach involves the following two assumptions:

- (i) The incident and final wave functions can be factored into a single-particle wave function times an internal wave function for the residual nucleus;
- (ii) The residual nucleus remains in the same internal state throughout the reaction. The spectator approximation assumes that the  $(A - 1)$  particle core remains in its ground state throughout the reaction.

In our calculation, we look at proton or neutron transitions leading to final states in  $^{12}\text{C}$ , for  $^{11}\text{B}$  or  $^{11}\text{C}$  targets, respectively (or the time-reversed reactions where the initial state is  $^{12}\text{C}$ ). We assume that the ground state of  $^{11}\text{B}$  may be represented by a  $(1p_{3/2})$  hole state, and that the final states populated in this reaction are the ground state of  $^{12}\text{C}$  (assumed to be a closed  $1p_{3/2}$  shell), and particle-hole states in  $^{12}\text{C}$  with a  $(1p_{3/2})$  hole. In the calculation of Tsai and Londergan<sup>43</sup> the  $^{11}\text{B}(p, \gamma)^{12}\text{C}$  transitions were estimated using the particle-hole amplitudes of Gillet and Vinh Mau<sup>45</sup> for states in  $^{12}\text{C}$ .

In Sec. III we review the qualitative features of the full  $(p, \gamma)$  spectrum predicted from TL. In this

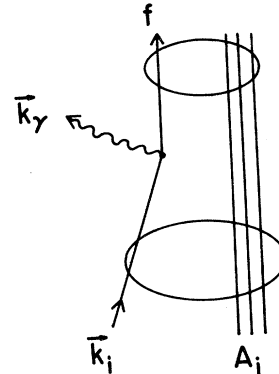


FIG. 3. Schematic picture of the direct-reaction model of radiative capture. An incident nucleon of momentum  $\vec{k}_i$  interacts with the target nucleus in state  $A_i$ . The nucleon emits a photon of momentum  $\vec{k}_\gamma$  and is captured into a single-particle shell model state  $f$ .

work, we concentrate on the transitions leading to the ground state of  $^{12}\text{C}$  and to high lying transitions in  $^{12}\text{C}$  with excitation energies 18.4–20.6 MeV (since these correspond to cross sections obtained by Blatt *et al.* at IUCF).<sup>39–41</sup> From particle-hole calculations in the  $A=12$  system we expect the  $(1d_{5/2})$ - $(1p_{3/2})^{-1}$  particle-hole strength to be concentrated in this excitation energy region in  $^{12}\text{C}$ . Inelastic scattering experiments have shown that both  $T=0$  and  $T=1$ ,  $4^-$  states in  $^{12}\text{C}$  appear at about 19.2–19.6 MeV excitation energy. As Donnelly and Walker<sup>46</sup> have stressed, the “stretched” particle-hole states built upon closed-shell nuclei are well represented by pure one particle-one hole con-

figurations. We expect to see much of the ( $p, \gamma$ ) reaction strength at these excitation energies leading to these stretched pure particle-hole configurations.

At the same time, however, we also expect to find a concentration of  $1^-$ ,  $2^-$ , and  $3^-$  excited states in  $^{12}\text{C}$  in this energy region. When we discuss our calculations of the radiative capture transitions and compare with the experimental data in Sec. III, we will examine two different simple estimates of the composition of the capture strength expected at these energies.

For the nuclear current operator  $\vec{j}(\vec{r})$  in Eq. (2.1), we take the one-body convection and spin magnetic currents, of the form

$$\vec{j}(\vec{r}) = e \sum_{\alpha=1}^A \left\{ \left[ \frac{1+\tau_3(\alpha)}{2iM_N} \right] \frac{1}{2} [\delta(\vec{r}_\alpha - \vec{r}) \vec{\nabla}_\alpha - \vec{\nabla}_\alpha \delta(\vec{r}_\alpha - \vec{r})] + \delta(\vec{r}_\alpha - \vec{r}) \frac{\mu_\alpha}{2M_N} \vec{\sigma}(\alpha) \times \vec{\nabla} \right\}. \quad (2.3)$$

In Eq. (2.6),  $\mu_\alpha$  is the nucleon magnetic moment in nuclear magnetons

$$\mu_\alpha = \frac{1+\tau_3(\alpha)}{2} \mu_p + \frac{1-\tau_3(\alpha)}{2} \mu_n, \quad (2.4)$$

where  $\mu_p = 2.79$ ,  $\mu_n = -1.91$ . With the spectator model for the nuclear states, using the one-body currents then involves taking the matrix element of the one-body current between an initial nucleon scattering state and a final single-particle nucleon wave function. We have written out the equations for these transition matrix elements and the multipole expansion of the electromagnetic potential in the Appendix. Performing an integration by parts for the electric multipole operator and using Siegert's theorem,<sup>47</sup> we replace the divergence of the one-body current by the matrix element of a one-body operator between initial and final nuclear wave functions. The magnetic multipole contributions are added separately to the electric multipole amplitudes.

For the relative wave function of a proton with the target nucleus, we used optical potentials relevant for the scattering of a nucleon from  $^{12}\text{C}$  (due to the scarcity of  $p + ^{11}\text{B}$  optical potentials in this energy region). The nucleon-nucleus potential is of the form

$$U(\vec{r}) = V_C(r) - \left[ V_0 f(r) + 4aW_D \frac{d}{dr} f(r) \right] + \frac{1}{m_\pi^2} V_{so} \frac{1}{r} \frac{d}{dr} f(r) \vec{L} \cdot \vec{\sigma}. \quad (2.5)$$

$V_C(r)$  is the Coulomb potential (the nuclear Coulomb potential is taken to be that due to a uniform sphere of charge of radius  $r_C A^{1/3}$ , where  $r_C = 1.25$  fm). The parameters  $V_0$ ,  $W_D$ , and  $V_{so}$  are taken from a potential used by Halderson and Philippot<sup>48</sup> to fit proton scattering from  $^{12}\text{C}$  in this energy region; they are listed in Table I. The form factor  $f(r)$  was a Woods-Saxon form, with radius  $r_0 = 1.25$  fm and diffuseness  $a = 0.55$  fm. For the final proton shell model state, we calculated the single-particle wave functions in a potential found by Birkholz<sup>11</sup> to be a good representation for describing the photodisintegration of  $^{12}\text{C}$  in a continuum shell model calculation around the giant dipole resonance region. The shell-model potential of Birkholz had the form of Eq. (2.8), with  $W_D = 0$ . The values of  $V_0$  and  $V_{so}$  are given in Table I.

The 19 MeV excited state in  $^{12}\text{C}$  is particle unbound, and the  $1d_{5/2}$  wave functions calculated with the Birkholz potential are not bound. As a result we should calculate the ( $p, \gamma_{19}$ ) reaction using a continuum wave function for the final proton single-particle state. In the calculation reported here, we used the Birkholz single-particle potential but we confined the wave function in a spherical box of ra-

TABLE I. Parameters for optical potentials used in this work. All strengths are in MeV, and radius and diffuseness parameters are in fm. The parameter  $W$  specified for the potential of Abdul-Jalil and Jackson is given by  $W = 10 + 0.14E_{c.m.} - 2 \times 10^6 E_{c.m.}^{-3}$ . For the value of  $W_V$  with that potential, the value specified was  $W_V = 1.2967W - 7.538$  or  $W_V = 0$ , whichever was larger.

	Halderson and Philpott (Ref. 48)	Birkholz (Ref. 11)	Abdul-Jalil and Jackson (Ref. 52)
$V_0$	$46 - 0.2 E_L$	70	$24.13 - 0.0866 E_{c.m.}$
$t_1$	1.25	1.151	1.454
$a_1$	0.55	0.57	0.554
$W_V$			$1.296 - 7.538$ (or zero)
$W_D$	3.19		$W - W_V$
$r_2$	1.25		0.932
$a_2$	0.55		0.612
$V_{so}$	6.26	5.5	$3.81 - 0.019 E_L$
$r_3$	1.25	1.151	$0.583 + 0.00274 E_L$
$a_3$	0.55	0.57	0.225
$W_{so}$			$-4.0 + 10.85 \exp(-0.0205 E_L)$
$r_4$			$1.83 - 0.00645 E_L$
$a_4$			$0.594 + 0.000616 E_L$

dus 10 fm. For these single particle states, the wave functions we use do not have the correct continuum behavior at large distances. This is a potentially serious deficiency in calculating radiative capture matrix elements, however, as we shall see in Sec. III, our results seem to agree with estimates of  $(p, \gamma)$  transitions which use more realistic continuum wave functions for the unbound final-state proton.<sup>48,49</sup>

### III. RESULTS AND DISCUSSION

The proton radiative capture measurements of Kovash *et al.* showed large transitions to states in  $^{12}\text{C}$  with excitation energy around 19 MeV. It was suggested by Arnold<sup>50</sup> that this might be the result of direct capture leading to particle-hole states in the residual nucleus. This was investigated by TL, who used bound and scattering states for a nucleon calculated with the shell model potential and residual interaction used by Birkholz. In TL, the final states were assumed to be one-particle one-hole states relative to a closed  $1p_{3/2}$  shell; the energies and particle-hole amplitudes for these states were taken from the random phase approximation (RPA) calculation of Gillet and Vinh Mau.<sup>45</sup>

If we restrict ourselves to the shell model wave function (i.e., wave functions calculated from the shell model potential only), then we obtain a spectrum of radiative capture strength corresponding to

each particle-hole excited state in  $^{12}\text{C}$ . In Fig. 4, we show the calculated transitions for  $^{11}\text{B}(p, \gamma)^{12}\text{C}$  vs the experimental data of Kovash *et al.*<sup>39,41</sup> for a proton incident energy of 40 MeV and a photon angle of  $60^\circ$ . In Fig. 4, the solid lines represent those states which are predominantly  $1d_{5/2}$  particle- $1p_{3/2}$  hole states (i.e., the coefficient for that state in the Gillet-Vinh Mau calculation is greater than 0.75). We see that the observed concentration of strength at about 19 MeV coincides with a concentration of  $1d_{5/2}$  single particle strength in a particle-hole picture.

Averaging the TL shell model results over the photon response of the detectors yielded a spectrum very similar to the experimental data, except that the magnitude (the dashed curve in Fig. 4) was only about  $\frac{1}{3}$  as large as the data. The shell model calculation corresponds to calculating the proton scattering waves in a purely real and quite deep ( $U \approx 70$  MeV) central potential. Radiative capture (or photodisintegration) cross sections depend strongly on the depth of the distorting potential<sup>44</sup>; thus increasing the depth of the potential decreases the predicted  $(p, \gamma)$  cross section.

The observed  $(p, \gamma)$  strength is consistent with radiative capture transitions to a group of particle-unbound excited particle-hole states in  $^{12}\text{C}$  which are predominantly  $1d_{5/2} - (1p_{3/2})^{-1}$  in character. These results suggest that a direct-reaction calculation with a conventional optical potential, which describes the elastic scattering of a proton from  $^{11}\text{B}$ ,

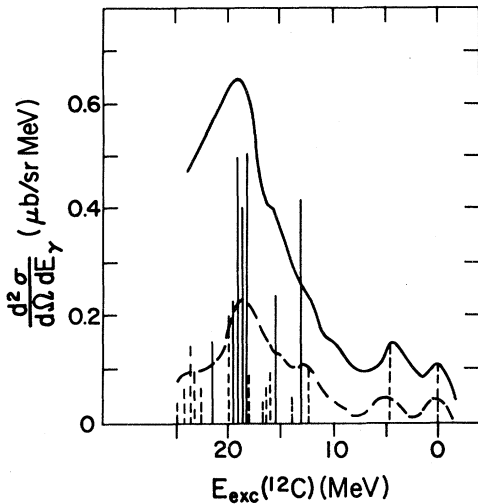


FIG. 4. The spectrum of photons emitted from  $^{11}\text{B}(p, \gamma)^{12}\text{C}$  for  $E_p = 40$  MeV and  $\theta = 60^\circ$ . Differential cross section ( $d^2\sigma/d\Omega dE_\gamma$ ) ( $\mu\text{b}/\text{sr}/\text{MeV}$ ) vs excitation energy in  $^{12}\text{C}$ . Solid curve: data of Kovash *et al.*, Ref. 39. Dashed curve: theory of Tsai and Londergan (TL), Ref. 43 including only the "shell model" or direct reaction term. Vertical lines show the excitation energies and relative magnitudes of the  $^{12}\text{C}$  particle-hole states used in the direct reaction  $(p, \gamma)$  cross sections of TL. The solid vertical lines represent those states which are predominantly  $(1d_{5/2})-(1p_{3/2})^{-1}$  states in  $^{12}\text{C}$ .

may reproduce both the magnitude and energy dependence of the experimental  $(p, \gamma)$  transitions. We investigate this possibility in this paper.

We have calculated the transitions  $^{11}\text{B}(p, \gamma_0)^{12}\text{C}$  and what we call  $^{11}\text{B}(p, \gamma_{19})^{12}\text{C}$ . We evaluate the ground state transition amplitude using an incident proton distorted wave, and a  $1p_{3/2}$  single-particle ground state calculated with the Birkholz shell model potential.<sup>11</sup> In Fig. 5 we show the differential cross section for the  $(p, \gamma_0)$  reaction versus proton laboratory energy  $E_p$  and the scattering angle  $\theta$  of the photon relative to the proton. To show the qualitative features of the  $(p, \gamma_{19})$  reaction, we have calculated a  $(p, \gamma)$  transition from a continuum proton to a  $1d_{5/2}$  single-particle final state, assuming that all of the  $1d_{5/2}$  strength is concentrated at 19.2 MeV excitation energy. This cross section is shown in Fig. 6.

The theoretical curves are given in 10 MeV intervals from 10–80 MeV proton energy. For the ground state transition, the 10 MeV cross section is dominated by  $E1$  transitions (the giant dipole resonance energy for the ground state occurs at  $E_p \sim 7$  MeV). All multipole transitions up to  $L=6$  are in-

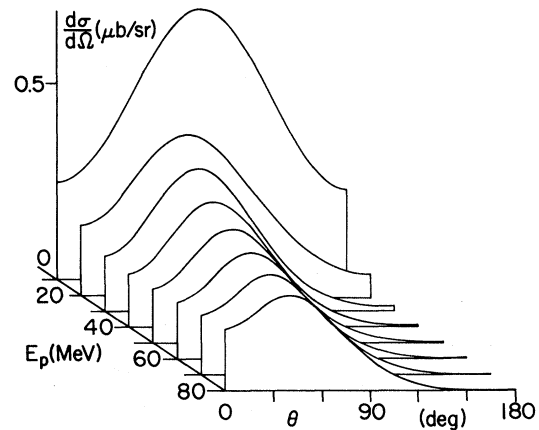


FIG. 5. Calculated differential cross section  $^{11}\text{B}(p, \gamma_0)^{12}\text{C}$  leading to the ground state of  $^{12}\text{C}$ . ( $d\sigma/d\Omega$ ) ( $\mu\text{b}/\text{sr}$ ) vs proton laboratory energy  $E_p$ , from 10–80 MeV and vs the scattering angle  $\theta$  of the photon relative to the incident proton direction. Curves are given every 10 MeV.

cluded to insure convergence at all energies. At higher energies the higher electric multipoles and the spin magnetization current contributions make the cross sections increasingly forward peaked in angle.

For the radiative capture transition to the  $1d_{5/2}$  single particle ( $1p_{3/2}$  hole) state in  $^{12}\text{C}$ , the calculated cross section exhibits a large peak at  $E_p \sim 21$  MeV. This peak is due primarily to  $E1$  transitions. At higher energies, the cross section decreases in magnitude and develops a strongly forward-peaked angular distribution, due to interference between  $E1$  and the higher electric multipole amplitudes.

Excitation functions have been obtained for a scattering angle of  $60^\circ$ , for both the ground state and "19 MeV" transitions, by Blatt *et al.*<sup>41–42</sup> The normalizations of these data have been checked by comparing with similar radiative capture data taken by Weller *et al.* at TUNL.<sup>51</sup> In Fig. 7, we compare our calculated excitation functions with the data. The " $(p, \gamma_{19})$ " data shown in Fig. 7 represent the sum of  $(p, \gamma)$  capture transitions leading to final states in  $^{12}\text{C}$  from excitation energy 18.4–20.6 MeV. As can be seen from Fig. 4, this excitation energy region contains several  $2^-$ ,  $3^-$ , and  $4^-$  excited states which are predicted to be dominated by  $1d_{5/2}$  single particle strength.

The theoretical  $(p, \gamma_{19})$  capture strength was calculated in two ways. First, we assumed that the experiment was measuring only transitions to the  $1d_{5/2}$  proton final state. This is just the capture cross sec-

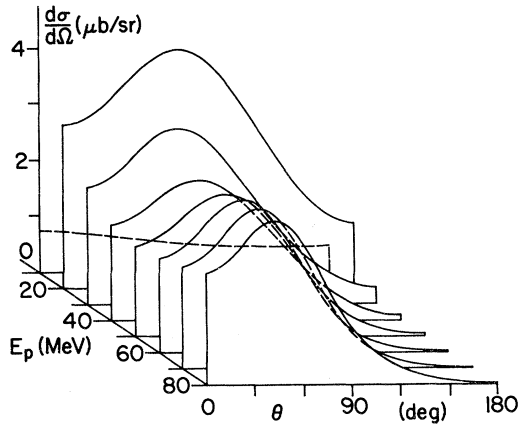


FIG. 6. Calculated differential cross section for  $^{11}\text{B}(p, \gamma_{19})^{12}\text{C}$ . The final states are the  $1d_{5/2}-(1p_{3/2})^{-1}$  particle-hole states in  $^{12}\text{C}$ , assumed to be degenerate at excitation energy 19.2 MeV. Notation is that of Fig. 4.

tion shown in Fig. 6. However, this will overestimate the experimental cross section since the residual interaction will fragment the  $1d_{5/2}$  strength into many states, and some of this strength would not be seen in the experimental energy range 18.4–20.6 MeV. As a simple estimate of the effects of fragmentation of the single-particle strength, we have multiplied our theoretical cross section by 0.8 (from TL,<sup>43</sup> we estimate that almost 80% of the  $1d_{5/2}$  radiative capture strength is found in this range of excitation energy in  $^{12}\text{C}$ ). This is shown as the solid curve in Fig. 7. As a second approximation, we took all of the particle-hole states in  $^{12}\text{C}$  from 18.4–20.6 MeV excitation as predicted by Gillet and Vinh Mau<sup>45</sup> (a mixture of  $1d_{5/2}$ ,  $1d_{3/2}$ , and  $2s_{1/2}$  particle states coupled to a  $1p_{3/2}$  hole), calculated the direct reaction ( $p, \gamma$ ) amplitudes to each state, and summed over all the states. This result is the dotted-dashed curve in Fig. 7.

The two predicted ( $p, \gamma_{19}$ ) curves are quite similar; the slightly different energy dependence reflects the fact that the dotted-dashed curves contain contributions from  $1d_{3/2}$  and  $2s_{1/2}$  single-particle wave functions, in addition to  $1d_{5/2}$  strength. The calculation correctly predicts a much larger ( $p, \gamma_{19}$ ) cross section than the ( $p, \gamma_0$ ) result, although the ( $p, \gamma_{19}$ ) theoretical curves overestimate the radiative capture strengths for  $E_p \gtrsim 50$  MeV. The direct-capture calculations fail to produce the energy dependence of the experimental excitation functions. The ( $p, \gamma_0$ ) cross section underestimates the data at low energies; the ( $p, \gamma_{19}$ ) theoretical cross section is smaller than the experimental data below 50 MeV and

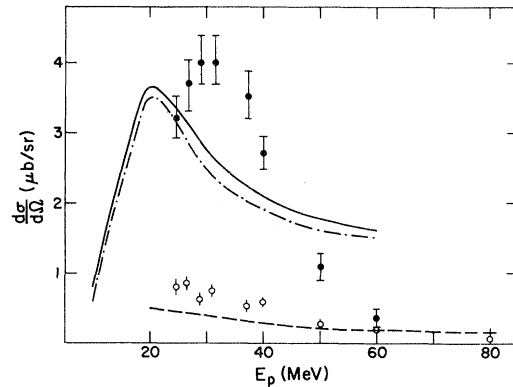


FIG. 7. Cross sections for  $^{11}\text{B}(p, \gamma_0)^{12}\text{C}$  and  $^{11}\text{B}(p, \gamma_{19})^{12}\text{C}$  vs proton energy  $E_p$  for scattering angle  $\theta_\gamma = 60^\circ$ . Data is from Blatt *et al.*, Refs. 41 and 42. Open circles:  $^{11}\text{B}(p, \gamma_0)^{12}\text{C}$  cross section. Solid circles:  $^{11}\text{B}(p, \gamma_{19})^{12}\text{C}$  cross section. Dashed curve: direct reaction calculation of  $^{11}\text{B}(p, \gamma_0)^{12}\text{C}$ . Solid curve: theoretical  $^{11}\text{B}(p, \gamma_{19})^{12}\text{C}$  cross section assuming the entire transition is to a  $1d_{5/2}$  single-particle state at 19.2 MeV excitation. Dotted-dashed curve:  $^{11}\text{B}(p, \gamma_{19})^{12}\text{C}$  cross section to summed particle-hole states in  $^{12}\text{C}$  between 18.4–20.6 MeV excitation using the  $^{12}\text{C}$  excitation energies and particle-hole amplitudes of Gillet and Vinh Mau, Ref. 45.

peaks at about 21 MeV, whereas the data has a maximum near 30 MeV.

One reason that our ( $p, \gamma_0$ ) result is too small is that we have not included the important “semi-direct” amplitudes which virtually excite the coherent set of particle-hole states which make up the giant dipole resonance (GDR) in  $^{12}\text{C}$ . “Semi-direct” amplitudes of the type shown in Fig. 8(b) are important in reproducing the location and shape of the giant dipole resonance. Consequently, we expect the direct reaction calculation to underestimate somewhat the ( $p, \gamma_0$ ) cross section, particularly in the vicinity of the GDR [ $E_p = 7$  MeV for the ( $p, \gamma_0$ ) transition].

For the ( $p, \gamma_{19}$ ) cross section, our calculation predicts neither the magnitude nor the shape of the  $60^\circ$  excitation function. There are several possible reasons for the disagreement between theory and experiment: (a) inadequacy of the optical potential used for the  $p + ^{11}\text{B}$  distortions; (b) the use of a bound state wave function to represent the unbound  $1d_{5/2}$  proton state; (c) overall normalization effects (either of the data or in the calculation); or (d) a more complicated reaction mechanism than we employed.

The shape of our ( $p, \gamma_{19}$ ) excitation function may be a result of using a  $1d_{5/2}$  single-particle wave

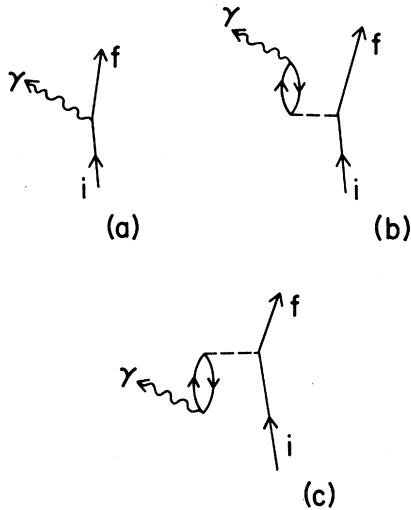


FIG. 8. Schematic diagram of important contributions to  $(p,\gamma)$  reactions in the vicinity of the giant dipole resonance region. (a) Direct reaction contribution; (b) and (c) "semidirect" reactions involving virtual excitation, via the residual interaction, of the coherent particle-hole states which make up the giant dipole resonance (GDR). This resonant state is then coupled to the photon. Diagram (b) dominates in the GDR region.

function confined to a spherical box of radius 10 fm, rather than using a continuum wave function for this state. This is unlikely, as we can compare our result with the energy dependence obtained by Halderson and Philpott,<sup>48,49</sup> who used continuum wave functions for the proton in particle-unbound final states. In Fig. 9 we plot the energy dependence of our results against the  $1d_{5/2}$  continuum results of Halderson and Philpott.<sup>49</sup> Both calculations agree quite well, and both give a maximum in the  $1d_{5/2}$  strength at an energy 8 or 9 MeV below the experimental peak; our approximation for the  $1d_{5/2}$  single-particle wave function gives a reasonable estimate of the shape of the  $(p,\gamma_{19})$  excitation function in this energy region.

Our theoretical  $(p,\gamma_{19})$  cross sections fail to reproduce the experimental  $60^\circ$  excitation functions. The peak occurs too low in energy and the magnitude of the  $(p,\gamma_{19})$  cross section is incorrect. This situation is similar to that which exists for direct-reaction  $(p,\gamma_0)$  calculations in the GDR region. The experimental  $(p,\gamma_0)$  peak occurs at a higher energy than that predicted by the direct capture model; the magnitude of the cross section at the resonance peak is larger than the prediction (in many nuclei, the experimental cross section is an order of magnitude larger than the direct-capture result). The energy

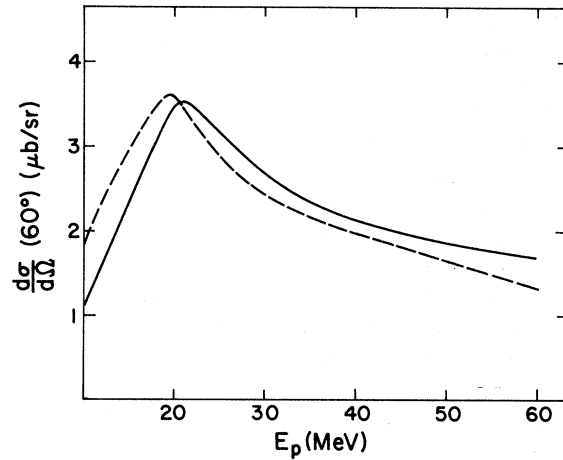


FIG. 9. Calculated energy dependence of the  $^{11}\text{B}(p,\gamma)$  reaction for  $\theta_\gamma=60^\circ$  leading to the  $(1d_{5/2})$  final proton state. Solid curve: our calculation using a  $d_{5/2}$  single particle wave function confined in a 10-fm spherical box. Dashed curve:  $1d_{5/2}$  strength obtained by Halderson and Philpott (Refs. 48 and 49) using a continuum  $d_{5/2}$  wave function.

dependence of the GDR also differs from the predictions of the direct-capture model.

This is understood as being due primarily to the coupling of the incident nuclear state to the GDR coherent particle-hole states, followed by radiative  $E1$  decay of the GDR state. Brown<sup>6</sup> first gave a simple schematic explanation of this effect, and it has since been corroborated by detailed calculations of the nuclear shell model in the continuum.<sup>10-16</sup> The situation is shown schematically in Fig. 8, where Fig. 8(a) represents the direct-capture mechanism and Fig. 8(b) gives the semidirect contribution for  $(p,\gamma)$  reactions. Assuming that all of the electric dipole strength is concentrated in a single state at  $1\hbar\omega$  excitation, then the *qualitative* effect of coupling to the giant dipole state can be taken into account by multiplying the  $E1$  contribution to the direct-capture amplitude by an enhancement factor<sup>6</sup>

$$M_{DSD}(E1) \sim M_D(E1) \left[ 1 + \frac{\Delta E}{E_\gamma - E_R + \frac{i\Gamma_R}{2}} \right]. \quad (3.1)$$

Here,  $M_{DSD}$  is the electric dipole amplitude including both the direct-capture part and the semidirect capture part and  $M_D$  is the direct-capture amplitude alone;  $\Delta E$  is the shift in energy of the di-

pole state from the average unperturbed particle-hole energy;  $E_R$  and  $\Gamma_R$  are the energy and width of the GDR; and  $E_\gamma$  is the photon energy.

Equation (3.1) gives a qualitative estimate of the effect of a concentration of  $E1$  strength at the excitation energy of  $E_R$  above the final state with a width  $\Gamma_R$ , in terms of an enhancement of the  $E1$  direct-capture amplitude. We have used Eq. (3.1) to see what enhancement of our  $E1$  direct-capture amplitude for the  $(p, \gamma_{19})$  reaction is necessary to make the  $60^\circ$  excitation function agree with the data. We have multiplied our calculated  $E1$  direct capture amplitudes for  $(p, \gamma_{19})$  by the direct-semidirect schematic model factor of Eq. (3.1) with  $\Delta E=4$  MeV,  $\Gamma_R=12$  MeV, and  $E_R=23$  MeV (i.e.,  $E_R$  corresponds to an excitation energy of about 42 MeV relative to the ground state of  $^{12}\text{C}$ ). We have left all other multipole amplitudes unchanged. In Fig. 10, we show the  $60^\circ$  excitation function both with and without this enhancement factor. The theoretical excitation function is now in very good agreement with the experimental data for incident proton energies below 50 MeV.

The angular distribution for  $E_p=28$  MeV is shown in Fig. 11. The solid curve is the theoretical angular distribution as calculated with no enhancement of the  $E1$  amplitude, and the dashed curve is

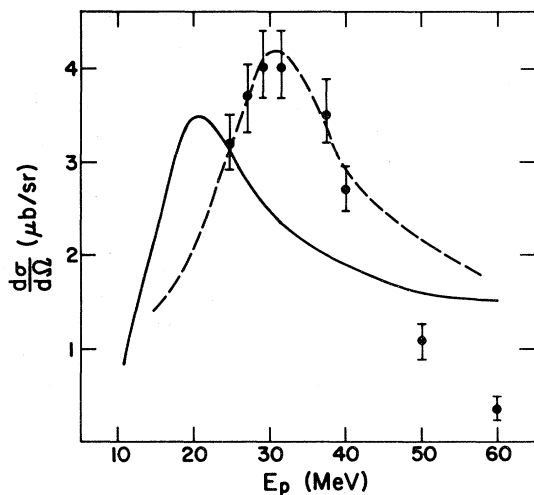


FIG. 10. Effect on the  $^{11}\text{B}(p, \gamma_{19})^{12}\text{C}$   $60^\circ$  excitation function of enhancing the theoretical transition amplitude. Circles: data of Refs. 41 and 42. Solid curve: theoretical calculation assuming transition to  $1d_{\frac{5}{2}}$  single-proton state at 19.2 MeV excitation. Dashed curve: result of enhancing the  $E1$  transition amplitude, via Eq. (3.1), using  $\Delta E=4$  MeV,  $E_R=23$  MeV, and  $\Gamma_R=12$  MeV.

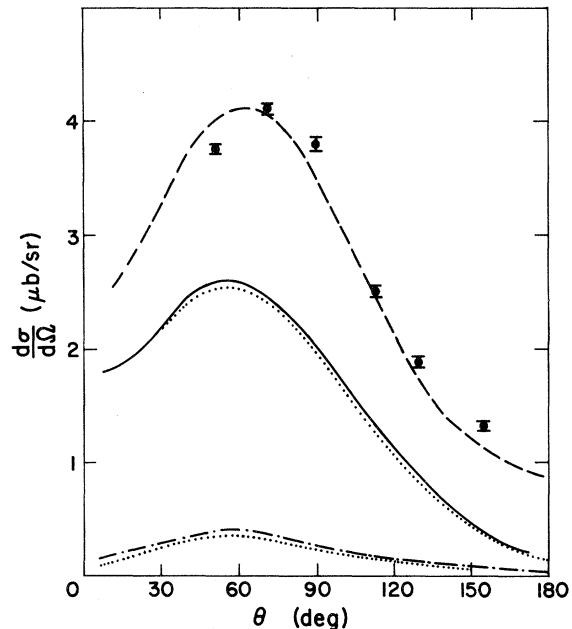


FIG. 11. Theoretical angular distributions for  $(p, \gamma)$  transitions on  $^{11}\text{B}$ , for proton incident energy 28.7 MeV. Dotted-dashed curve:  $^{11}\text{B}(p, \gamma_0)^{12}\text{C}$ . Solid and dashed curves:  $^{11}\text{B}(p, \gamma_{19})^{12}\text{C}$ , same notation as Fig. 10. The dotted curves are the cross sections calculated with the electric multipoles only, and show the size of the effects of the spin magnetization current on the  $(p, \gamma)$  cross sections at this energy. Data are from Refs. 41 and 42.

the result when we enhance our  $(p, \gamma_{19})$   $E1$  amplitude. The angular distribution is noticeably altered by enhancing the  $E1$  amplitude. This is because the  $E1$ - $E2$  interference is primarily responsible for changing the shape of the observed angular distribution, and is strongly affected by increasing the relative strength of the  $E1$  contribution. The dots are the experimental data.<sup>42</sup> The fits to both the  $60^\circ$  excitation function and the angular distribution at 28.7 MeV are noticeably improved when we increase the theoretical  $E1$  amplitude by this factor.

To show that the contributions from magnetic multipole transitions are relatively unimportant, we have also calculated the differential cross sections neglecting the spin magnetization current contributions and the magnetic multipole part of the convection current. These are shown as the dotted curves in Fig. 11. We see that at a proton energy of 28.7 MeV, the magnetic contributions are rather small at all angles. We have included the theoretical angular dependence of the  $(p, \gamma_0)$  cross section in Fig. 11 (the dotted-dashed curve).

At somewhat higher energies, we compare the

direct capture model results with the cross sections of the time-reversed reaction  $^{12}\text{C}(\gamma, p_0)^{11}\text{B}$  as measured at Glasgow by Matthews *et al.*<sup>28</sup> (Fig. 12). For a photon incident energy  $E_\gamma$  of 60 MeV, our calculated forward-angle cross sections are smaller than the data but agree with the experimental cross sections for  $\theta \geq 90^\circ$ . At  $E_\gamma = 80$  MeV, the forward-angle cross sections agree with the data, but the back-angle cross sections tend to be too high. As with the  $(p, \gamma)$  transitions, our calculations are qualitatively correct but do not reproduce the energy dependence of  $d\sigma/d\Omega$  for fixed scattering angle.

As the energy increases, the spin magnetization currents play an increasingly important role in the photonuclear reaction. The dotted-dashed line in Fig. 12 gives the result of neglecting the one-body spin-magnetization current in these reactions. At forward and backward scattering angles, the spin magnetization current accounts for about  $\frac{1}{3}$  of the total  $(\gamma, p_0)$  transition.

We have calculated the radiative capture transitions using a different potential to describe the proton scattering wave, in order to estimate the dependence of our results upon the description of the continuum proton wave function. We used the optical potential of Abdul-Jalil and Jackson<sup>52</sup> which was obtained by fitting proton scattering and polarization data from light nuclei in the energy range 50–160 MeV. The optical potential of Abdul-Jalil and Jackson had the form

$$V(r) = V_C(r) - V_0(r)f_1(r) - i \left[ W_V f_2(r) - 4a_2 W_D \frac{d}{dr} f_2(r) \right] + \frac{1}{m_\pi^2 r} \left[ V_{\text{so}} \frac{d}{dr} f_3(r) + i W_{\text{so}} \frac{d}{dr} f_4(r) \right] \vec{l} \cdot \vec{\sigma}. \quad (3.2)$$

In Eq. (3.2),  $V_C(r)$  is the Coulomb potential, and each  $f_i(r)$  is a Woods-Saxon potential

$$f_i(r) = \left[ 1 + \exp \left( \frac{r - R_i}{a_i} \right) \right]^{-1}, \quad (3.3)$$

$$R_i \equiv r_i A^{1/3}.$$

The values of the strengths, radii, and diffuseness for the 13 parameters in these potentials are given in Table I. With these potentials, the real and imaginary spin-orbit potentials have quite different shapes.

The results are shown versus the  $^{12}\text{C}(\gamma, p_0)^{11}\text{B}$  data in Fig. 11; the dashed line gives the photonuclear transitions calculated using the Abdul-Jalil

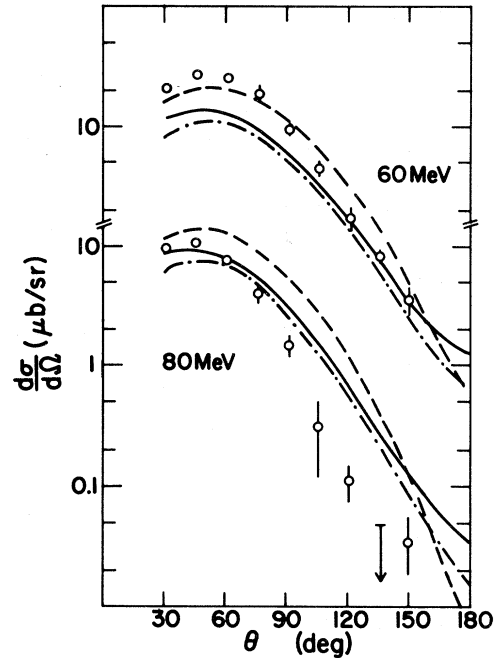


FIG. 12. Photodisintegration reaction  $^{12}\text{C}(\gamma, p_0)^{11}\text{B}$  vs proton scattering angle  $\theta$ , for incident proton energies 60 and 80 MeV. Data is that of Matthews *et al.*, Ref. 28. Solid curve: theoretical calculation; dotted-dashed curve: theoretical calculation using convection current only (neglecting spin magnetization current). Dashed curve: calculation using the optical potential of Abdul-Jalil and Jackson (Ref. 52) to describe the proton scattering.

and Jackson potential for the  $p + ^{11}\text{B}$  scattering. The cross sections calculated with this potential tend to be larger at forward scattering angles than those using the Halderson-Philpott potential; at some angles the difference is as large as a factor of 2. Although both potentials give results which are in qualitative agreement with the data, neither potential reproduces the quantitative behavior of the photonuclear cross sections at both energies (although the Abdul-Jalil-Jackson potential gives good agreement with the data at  $E_\gamma = 60$  MeV).

We find that the  $(\gamma, p_0)$  cross sections calculated with two different optical potentials but the same bound-state wave functions produce results which differ by as much as a factor of 2 at some angles.

Our results are similar to those of Boffi *et al.*,<sup>53</sup> who used various combinations of optical potentials and bound state wave functions in direct reaction calculations of  $(\gamma, p_0)$  reactions on light closed shell nuclei. They found even larger variations (sometimes greater than a factor of 5) in the  $(\gamma, p_0)$  cross sections calculated with different combinations of bound state and scattering wave functions. Fink, Hebach, and Kummel<sup>44</sup> first pointed out the strong sensitivity of the photonuclear reactions to the choice of bound state and scattering single-particle wave functions in a direct-reaction calculation.

We have also calculated the  $^{12}\text{C}(\gamma, n_0)^{11}\text{C}$  cross sections in the same direct-reaction model. We use the effective charges for the neutron in the  $l$ th electric multipole amplitude

$$e_n(l) = e \left[ -\frac{Z}{A} \right]^l. \quad (3.4)$$

For  $A=12$ , this c.m. effective charge is negligible for all but the  $E1$  multipoles. In addition, we have the contribution from the neutron spin magnetization current. Our results are shown in Fig. 13 for  $\gamma$  energies 63 and 79 MeV. The data are those of Schier and Schoch.<sup>32</sup> At large scattering angles, our results are of the same magnitude as the data; however, the direct-reaction calculation completely fails

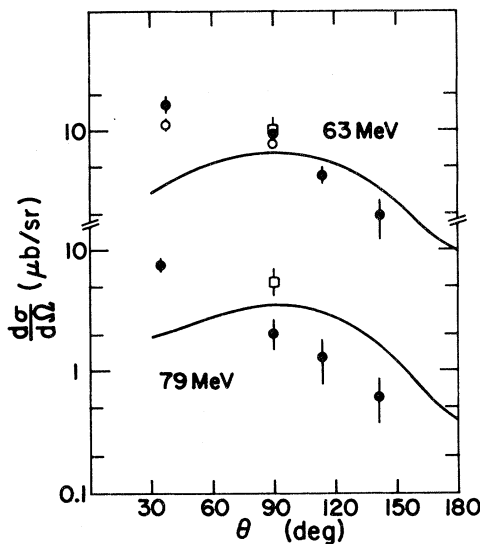


FIG. 13. Photoneutron reaction  $^{12}\text{C}(\gamma, n_0)^{11}\text{C}$  vs neutron scattering angle  $\theta$ , for incident photon energies 63 and 79 MeV. Data is that of Schier and Schoch, Ref. 32.

to reproduce the large forward-angle  $(\gamma, n_0)$  cross sections observed by Schier and Schoch. Neither the magnitude nor the shape of the  $(\gamma, n_0)$  cross section is reproduced by the direct-reaction model.

We emphasize this because the failure of the direct-reaction picture to adequately explain the  $(\gamma, n_0)$  results implies that an important nondirect reaction mechanism is present in both the  $(\gamma, p)$  and  $(\gamma, n)$  reactions (at least for photon energies of 50 MeV or greater). This casts doubt on the direct-reaction analyses of  $(\gamma, p_0)$  reactions,<sup>30,53</sup> and even  $(e, e'p)$  reactions<sup>54</sup> at these energies. Such analyses have attempted to connect the  $(\gamma, p_0)$  reactions to the proton single-particle momentum density via the direct-reaction picture. In this light, the large and forward-peaked  $(\gamma, n)$  measurements on  $^{12}\text{C}$  and  $^{16}\text{O}$  provide a persuasive argument for the importance of semidirect contributions to the  $(\gamma, N)$  reaction at intermediate energies. This has been emphasized by Hebach, Wortberg, and Gari.<sup>33-35</sup>

#### IV. CONCLUSIONS

We have examined a direct-reaction model for nucleon radiative capture and the time-reversed photonuclear reaction. In this model, the nucleon radiates a photon in the presence of the strong nuclear field, and we take the matrix elements of the one-body convective current and spin magnetization operators between a distorted wave for the incident nucleon and a single-particle shell model state for the captured nucleon. We have applied this model to the proton radiative capture transitions on  $^{11}\text{B}$ , leading either to the ground state of  $^{12}\text{C}$  or to a band of excited states in  $^{12}\text{C}$  between 18.4 and 20.6 MeV excitation. Particle-hole calculations of simple excited states in  $A=12$  show that this excitation region should be populated by a number of excited states which are predominantly  $(1d_{5/2})-(1p_{3/2})^{-1}$  in character. We have calculated the proton radiative capture cross sections using two different simple models for the excited states being populated in the  $(p, \gamma_{19})$  reaction. We have also examined the validity of this model for describing photoproton and photoneutron decays of  $^{12}\text{C}$  [i.e.,  $^{12}\text{C}(\gamma, p_0)^{11}\text{B}$  and  $^{12}\text{C}(\gamma, n_0)^{11}\text{C}$ ].

This model does reproduce the qualitative features of these transitions, but it does fail in some respects:

(i) The quantitative behavior of the excitation functions is not well reproduced. For the  $(p, \gamma_{19})$

transitions in  $^{11}\text{B}$ , the direct reaction model predicts a peak in the  $60^\circ$  cross section at  $E_p \sim 21$  MeV, whereas the experimental result peaks at about 29 MeV. For our calculation, we showed that the discrepancy between our result and the data seems to be consistent with the existence of additional  $E1$  strength (relative to the  $1d_{5/2}^+$  component of particle-hole excited states in  $^{12}\text{C}$ ) at an excitation energy of about 42 MeV in  $^{12}\text{C}$ . This additional strength would not have been included in our direct-reaction calculation.

(ii) The magnitude and shape of the  $^{12}\text{C}(\gamma, n_0)^{11}\text{C}$  cross sections cannot be reproduced by the direct-reaction model. The calculated cross sections are too small by a factor of 4–5 in the forward direction.

The large experimental  $(\gamma, n_0)$  cross sections provide strong evidence for the importance of semi-direct processes in radiative capture transitions. Hebach *et al.*<sup>33–35</sup> have pursued this idea; they suggest that the two-body current amplitudes are large and can explain the  $(\gamma, p_0)$  and  $(\gamma, n_0)$  data in a rather natural way. It would be very useful to obtain  $(n, \gamma)$  data in the region of the IUCF measurements (20–60 MeV), leading both to the ground state of the residual nuclei but also to the important excited particle-unbound states analogous to the  $(p, \gamma)$  transition observed on a  $^{11}\text{B}$  target. Above the GDR energy region, theoretical direct reaction calculations tend to predict that  $(n, \gamma)$  cross sections should be dramatically different from  $(p, \gamma)$  in both magnitude and angular distribution; consequently, comparing  $(p, \gamma)$  and  $(n, \gamma)$  measurements could be very useful in determining the adequacy of a direct-reaction treatment of radiative capture.

The theoretical  $(p, \gamma)$  direct reaction cross sections are of the same magnitude as the experimental data, so the direct amplitude must be an important part of the full radiative capture process in light nuclei. Our calculations suggest that the  $(p, \gamma)$  and  $(\gamma, p)$  amplitudes have variations of roughly a factor of 2 between different realistic bound and scattering wave functions for the proton.

#### ACKNOWLEDGMENTS

This research was supported in part by the National Science Foundation. We would like to thank Prof. S. L. Blatt for allowing us to use the preliminary  $(p, \gamma)$  cross sections. We acknowledge very useful conversations with H. R. Weller, M. Kovash, and D. Halderson.

#### APPENDIX: EVALUATION OF ELECTROMAGNETIC TRANSITION AMPLITUDES

The photon electromagnetic potential  $\vec{A}_\lambda(\vec{r})$  for helicity  $\lambda$ , defined in Eq. (2.2), can be separated into electric and magnetic multipole operators. The potential can then be written as

$$\vec{A}_\lambda(\vec{r}) = -\frac{2\pi}{\sqrt{\omega_\gamma}} \sum_{L,M} (-i)^L \hat{L} (-1)^\lambda D_{M,-\lambda}^L(-\phi, -\theta, \phi) \times (\vec{E}_{LM} - \lambda \vec{M}_{LM}). \quad (\text{A1})$$

In Eq. (A1),  $D_{M,-\lambda}^L$  is the rotation operator (we use the phase convention of Brink and Satchler,<sup>55</sup> and Messiah<sup>56</sup>), and the Euler angles  $(\theta, \phi)$  are the angles of the photon momentum  $\vec{k}_\lambda$  relative to the axis of quantization. We use  $\hat{L} \equiv (2L+1)^{1/2}$ .

The multipole operators  $M_{LM}$  and  $E_{LM}$  are defined by

$$\vec{M}_{LM} = j_L(k_\gamma r) \vec{Y}_{LL1}^M(\hat{r}), \quad (\text{A2})$$

$$\vec{E}_{LM} = \frac{1}{k_\gamma} \vec{\nabla} \times [j_L(k_\gamma r) \vec{Y}_{LL1}^M(\hat{r})]. \quad (\text{A3})$$

In Eqs. (A2) and (A3),  $\vec{Y}_{LL1}^M$  are the vector spherical harmonics. In order to evaluate the matrix elements of the electric multipole operator, it is useful to split the electric multipole operator into two parts. We write

$$\vec{E}_{LM} \equiv \vec{E}_{LM}^{(1)} + \vec{E}_{LM}^{(2)}, \quad (\text{A4})$$

$$\vec{E}_{LM}^{(1)} = \frac{i}{\sqrt{L(L+1)}} \vec{\nabla} [Q_L(k_\gamma r) Y_{LM}(\hat{r})], \quad (\text{A5})$$

$$\vec{E}_{LM}^{(2)} = \frac{i}{\sqrt{L(L+1)}} k_\gamma \vec{r} j_L(k_\gamma r) Y_{LM}(\hat{r}), \quad (\text{A6})$$

$$Q_L(x) \equiv \left[ 1 + x \frac{d}{dx} \right] j_L(x).$$

For the energies which we are interested in, the contribution to the radiative capture amplitudes from  $E_{LM}^{(2)}$  is typically only a few percent of the total  $(p, \gamma)$  cross section.

For  $(p, \gamma)$  reactions, we want to evaluate the transition amplitude of Eq. (2.1),

$$M_{fi}^{(\lambda)} = - \int d\vec{r} \langle \psi_f | \vec{j}(\vec{r}) | \psi_i \rangle \cdot \vec{A}_\lambda(\vec{r}). \quad (\text{A7})$$

In Eq. (A7),  $|\psi_f\rangle$  is the final nuclear state (as-

sumed to be a proton in a single-particle shell model state relative to the initial core) and  $|\psi_i\rangle$  is a wave function describing a continuum proton scattering from the initial nuclear target. We used the one-body convection current and spin magnetization

$$\vec{j}_c(\vec{r}) = e \sum_{\alpha=1}^A \left[ \frac{1 + \tau_3(\alpha)}{2iM_N} \right] \frac{1}{2} [\delta(\vec{r}_\alpha - \vec{r}) \vec{\nabla}_\alpha - \vec{\nabla}_\alpha \delta(\vec{r}_\alpha - \vec{r})], \quad (\text{A9})$$

$$\vec{j}_m(\vec{r}) = e \sum_{\alpha=1}^A \delta(\vec{r}_\alpha - \vec{r}) \frac{\mu_\alpha}{2M_N} \vec{\sigma}(\alpha) \times \vec{\nabla}. \quad (\text{A10})$$

Since the operator  $E_{LM}^{(1)}$  is the gradient of the function  $Q_L(k_\gamma r) Y_{LM}(\hat{r})$ , we integrate Eq. (A7) by parts and use the current conservation identity

$$\begin{aligned} \vec{\nabla} \cdot \vec{j}(r) &= - \frac{\partial \rho(\vec{r})}{\partial t} \\ &= -i [H_N, \rho(\vec{r})] \end{aligned} \quad (\text{A11})$$

as was used by Siegert.<sup>47</sup>

In Eq. (A11),  $\rho(\vec{r})$  is the nuclear charge density and  $H_N$  is the nuclear Hamiltonian. In evaluating Eq. (A11), we use the fact that  $|\psi_i\rangle$  and  $|\psi_f\rangle$  are eigenfunctions of the nuclear Hamiltonian with eigenenergies related by

$$E_i = E_f + k_\gamma, \quad (\text{A12})$$

for the nuclear charge density  $\rho(r)$  we use the *point charge density*

$$\rho_{\text{pt}}(\vec{r}) = e \sum_{\alpha=1}^A \left[ \frac{1 + \tau_3(\alpha)}{2} \right] \delta(\vec{r} - \vec{r}_\alpha). \quad (\text{A13})$$

The matrix elements of the operators  $\vec{E}_{LM}^{(2)}$  and  $\vec{M}_{LM}$  are then calculated directly and added to the matrix elements of  $\vec{E}_{LM}^{(1)}$  calculated as described here.

In our direct reaction model, we have assumed that the target nucleus acts as a spectator during the interaction, and we have used only the matrix elements of the one-body convection and magnetic currents. Consequently, we need to evaluate the transition amplitude between an initial scattering state for the relative proton-nucleus wave function and a final single particle shell model state (assumed to be bound in a Woods-Saxon potential).

current

$$\vec{j}(\vec{r}) = \vec{j}_c(\vec{r}) + \vec{j}_m(\vec{r}), \quad (\text{A8})$$

where

The scattering wave function for the initial state is expanded in partial waves to give the relative  $p$ -nucleus wave function

$$\begin{aligned} \chi_{i;\mu}^{(+)}(\vec{r}) &= \sqrt{4\pi} \sum_l i^l \hat{J}(-1)^{l-1/2+\mu} \\ &\times \begin{pmatrix} l & \frac{1}{2} & j \\ 0 & \mu & -\mu \end{pmatrix} \frac{R_{lj}(r)}{k_i r} [Y_l(\hat{r}) \chi_{1/2} J_{j\mu}] \end{aligned} \quad (\text{A14})$$

In Eq. (A14), the axis of quantization has been taken to be the incident momentum  $k_i$ . Similarly, we can write the wave function for a single-particle shell model state with total angular momentum  $(J, M)$ , orbital angular momentum  $l$ , and additional quantum numbers  $\alpha$  as

$$\chi_f(r) = u_{njl}(r) [Y_l(\hat{r}) \chi_{1/2}]_{JM}. \quad (\text{A15})$$

In our calculation, the  $1d_{5/2}$  single particle states are actually unbound, but we normalized them in a 10-fm spherical box in order to facilitate calculations. With these definitions for the scattering and bound state wave function, we can then straightforwardly calculate the matrix elements of the one-body convection and spin-magnetization currents. We divide the convection current up into its electric and magnetic multipole moments, and we further divide the electric multipole operator into two parts via Eqs. (A4)–(A6). The largest piece is the operator  $E_{LM}^{(1)}$ , which we evaluate by using the current conservation identity and the point charge density as described in Eqs. (A8)–(A13). This leads to the following expression for the matrix elements of the one body convection current

$$\begin{aligned} M_{\text{fi},c}(E^{(1)}) &= \frac{-2\pi e}{k_i [k_\gamma]^{1/2}} \sum_{LM} (-)^M \tilde{e}_L D_{M,-\lambda}^L(\hat{k}_\gamma) \\ &\times \sum_{\{p\},lj} \rho_{\text{fi}}(p) G_0^e \left[ \frac{(2L+1)}{\sqrt{L(L+1)}} \begin{pmatrix} l_p & L & l \\ 0 & 0 & 0 \end{pmatrix} \right] F^{(1)}(p, l, j, L). \end{aligned} \quad (\text{A16})$$

In Eq. (A16),  $\{p\}$  represents the quantum numbers  $(n_p, l_p, j_p, m_p)$  of the single-particle proton final state, and  $u_p = u_{n_p l_p j_p}(r)$ . The coefficient  $\rho_{fi}$  represents the spin-isospin coupling from the initial nuclear target, with spin and isospin  $(J_i, M_i)$  and  $(T_i, T_{3i})$ , respectively, to the final state of proton plus nucleus with total spin and isotopic spin  $(J_f, M_f)$  and  $(T_f, T_{3f})$ :

$$\rho_{fi}(p) = (-)^{T_i - 1/2 + T_{3f}} \hat{T}_f \begin{bmatrix} T_i & \frac{1}{2} & T_f \\ T_{3i} & t_{3p} & -T_{3f} \end{bmatrix} \\ \times (-)^{J_i - j_p + M_f} \hat{J}_f \begin{bmatrix} J_i & j_p & J_f \\ M_{fi} & m_p & -M_f \end{bmatrix}. \quad (\text{A17})$$

$G_0^c$  is a geometric factor defined by

$$G_0^c = (-i)^{L+1} \hat{j}_p \hat{l}_p (2J+1)(2l+1) \\ \times \begin{bmatrix} l & \frac{1}{2} & J \\ 0 & \mu & -\mu \end{bmatrix} \begin{bmatrix} J & L & j_p \\ \mu & M & -m_p \end{bmatrix} \begin{bmatrix} J & L & j_p \\ l_p & \frac{1}{2} & l \end{bmatrix}. \quad (\text{A18})$$

The radial matrix element  $F^{(1)}$  is given by

$$F^{(1)}(p, lJ, L) = \int_0^\infty dr r u_p(r) Q_L(k_\gamma r) R_{lJ}(r). \quad (\text{A19})$$

Note that in Eq. (A16), we have used the c.m.-

$$M_{fi;c}^{(2)}(E^{(2)}) = \frac{-2\pi e}{k_i [k_\gamma]^{1/2}} \sum_{LM} (-)^M \tilde{e}_l D_{M, -\lambda}^L(\hat{k}_\gamma) \\ \times \sum_{\{p\}, lJ} \rho_{fi}(p) G_0^c \left[ \frac{-k_\gamma}{M_N} \right] [C_+ F_+^{(2)}(p, lJ, L) + C_- F_-^{(2)}(p, lJ, L)]. \quad (\text{A21})$$

Here we define the quantities

$$F_\pm^{(2)}(p, lJ, L) = \int_0^\infty dr r^2 V_\pm(r) j_L(k_\gamma r) R_{lJ}(r) \quad (\text{A22})$$

with

$$V_+(r) = \frac{\sqrt{l_p+1}}{2l_{p+1}} \left[ \frac{l_p}{r} - \frac{d}{dr} \right] u_p(r), \\ V_-(r) = \frac{\sqrt{l_p}}{2l_{p+1}} \left[ \frac{l_{p+1}}{r} + \frac{d}{dr} \right] u_p(r), \\ C_+ = -\frac{\sqrt{2L+1}}{L} G_{1,1}(l_p, L, l) + \frac{\sqrt{2L+1}}{L+1} G_{1,-1}(l_p, L, l), \\ C_- = -\frac{\sqrt{2L+1}}{L} G_{-1,1}(l_p, L, l) + \frac{\sqrt{2L+1}}{L+1} G_{-1,-1}(l_p, L, l), \quad (\text{A23})$$

corrected effective charge for the  $L$ th electric multipole

$$\tilde{e}_L = \left[ \frac{1+\tau_3}{2} \right] \left[ \left[ 1 - \frac{1}{A} \right]^L - \left[ -\frac{1}{A} \right]^L \right] + Z \left[ -\frac{1}{A} \right]^L, \quad (\text{A20})$$

for a nucleus with charge  $Z$  and atomic number  $A$ , and  $\tau_3 = +1$  for a proton and  $(-1)$  for a neutron. The effective charge  $\tilde{e}_L$  has been derived from long wavelength arguments and may not be adequate for the energies examined in this work. For comparison with other work, Halderson and Philpott<sup>48</sup> do not use an effective charge but instead replace the convection contribution from the proton and a coherent contribution from the nuclear target (with charge  $Z$  and mass  $A$ ). This allows them to use physical charges for both projectile and target but replaces the sum over target proton coordinates with a coherent convective contribution from the target. Boffi *et al.*<sup>53</sup> simply use the proton charge  $(-e)$  for all multipoles (they are interested in higher energies than we consider). For our case ( $p + {}^{11}\text{B}$ ), our approximation of using effective charges is essentially identical to that of Boffi *et al.* for all multipoles except for  $E1$  amplitude.

The remaining electric and magnetic matrix elements of the convection current can be calculated

$$G_{\mu,\nu}(L_a, L_b, L_c) \equiv \sqrt{2L_a + 2\mu + 1} \sqrt{2L_b + 2\nu + 1} \begin{bmatrix} L_a + \mu & L_b + \nu & L_c \\ 0 & 0 & 0 \end{bmatrix} \begin{bmatrix} L_a + \mu & L_b + \nu & L_c \\ L_b & L_a & 1 \end{bmatrix},$$

$$M_{\text{fi},c}(M) = -\frac{2\pi e}{k_i [k_\gamma]^{1/2}} \frac{\lambda}{M_N} \sum_{LM} (-)^M \tilde{e}_L D_{M,-\lambda}^L(\hat{k}_\gamma) (2L+1) \\ \times \sum_{\{p\}, IJ} \rho_{\text{fi}}(p) G_0^s(-i) [F_+^{(M)} G_{1,0}(I_p, L, I) + F_-^{(M)} G_{-1,0}(I_p, L, I)], \quad (\text{A24})$$

$$F_{\pm}^M \equiv \int_0^\infty r dr V_{\pm}(r) j_L(k_\gamma r) R_{IJ}(r). \quad (\text{A25})$$

Finally, the spin magnetization current contributions can be written

$$M_{\text{fi},s} = \frac{2\pi e}{k_i [k_\gamma]^{1/2}} \lambda \sqrt{3} \mu (\tau_3) \frac{k_\gamma}{M_N} \sum_{LM, L'} (-)^M D_{M,-\lambda}^L(\hat{k}_\gamma) \sum_{\{p\}, IJ} \rho_{\text{fi}}(p) G_0^s F_S(p, IJ, L'), \quad (\text{A26})$$

where

$$F_S(p, IJ, L') \equiv \int_0^\infty dr r u_p(r) j_{L'}(k_\gamma r) R_{IJ}(r), \quad (\text{A27})$$

and

$$G_0^S = (-1)^{L+j_p-1/2} (i)^{l+L'} (2L+1)(2L'+1)(2l+1)(2J+1) \hat{l}_p \hat{j}_p \\ \times \begin{bmatrix} 1 & L' & L \\ -\lambda & 0 & \lambda \end{bmatrix} \begin{bmatrix} l & \frac{1}{2} & J \\ 0 & \mu & -\mu \end{bmatrix} \begin{bmatrix} J & L & j_p \\ \mu & M & -m_p \end{bmatrix} \begin{bmatrix} l_p & L' & l \\ 0 & 0 & 0 \end{bmatrix} \begin{bmatrix} \frac{1}{2} & \frac{1}{2} & 1 \\ l_p & l & L' \\ j_p & J & L \end{bmatrix}. \quad (\text{A28})$$

<sup>1</sup>S. S. Hanna, in *Proceedings of the Topical Conference on Giant Multipole Resonances, Oak Ridge, Tennessee, 1979*, edited by F. Bertrand (Harwood, New York, 1979), and references therein.

<sup>2</sup>K. A. Snover, in *Proceedings of the Topical Conference on Giant Multipole Resonances, Oak Ridge, Tennessee, 1979*, edited by F. Bertrand (Harwood, New York, 1979), and references therein.

<sup>3</sup>S. S. Hanna, in *Proceedings of the International Conference on Nuclear Physics with Electromagnetic Interactions, Mainz, 1979*, edited by H. Arenhovel and D. Drechsel (Springer, New York, 1979), and references; J. Speth, *ibid.*

<sup>4</sup>S. S. Hanna, in *Charged-Particle-Induced Radiative Capture* (International Atomic Energy Agency, Vienna, 1974).

<sup>5</sup>A. M. Lane, Nucl. Phys. **11**, 625 (1959); A. M. Lane and J. E. Lynn, *ibid.* **11**, 646 (1959); **17**, 563 (1960); **17**, 586 (1960).

<sup>6</sup>G. E. Brown, Nucl. Phys. **57**, 339 (1964).

<sup>7</sup>C. F. Clement, A. M. Lane, and J. A. Rook, Nucl. Phys. **66**, 273 (1965); **66**, 293 (1965).

<sup>8</sup>A. A. Lushnikar and D. F. Zaretsky, Nucl. Phys. **66**, 35

(1965).

<sup>9</sup>F. Cvelbar and S. L. Whetstone, in *Charged-Particle-Induced Radiative Capture* (IAEA, Vienna, 1974), and references.

<sup>10</sup>B. Buck and A. D. Hill, Nucl. Phys. **A95**, 271 (1967).

<sup>11</sup>J. Birkholz, Nucl. Phys. **A189**, 385 (1972).

<sup>12</sup>M. Marangoni and A. M. Saruis, Nucl. Phys. **A132**, 649 (1969).

<sup>13</sup>C. Mahaux and A. M. Saruis, Nucl. Phys. **A177**, 103 (1971).

<sup>14</sup>M. Marangoni, P. O. Ottaviani, and A. M. Saruis, CERN Report CERN, RT/FI, 1976, p. 10.

<sup>15</sup>C. M. Shakin and W. L. Wang, Phys. Rev. Lett. **26**, 902 (1971); W. L. Wang and C. M. Shakin, Phys. Rev. **C 9**, 2144 (1974).

<sup>16</sup>D. G. Mavis, Ph.D. thesis, Stanford University, 1977 (unpublished).

<sup>17</sup>F. S. Dietrich and A. K. Kerman, Phys. Rev. Lett. **43**, 114 (1979); M. Potokar, Phys. Lett. **92B**, 1 (1980).

<sup>18</sup>R. G. Allas, S. S. Hanna, L. Meyer-Schutzmeister, and R. E. Segel, Nucl. Phys. **58**, 122 (1964).

<sup>19</sup>H. F. Glavish, S. S. Hanna, R. Avida, R. N. Boyd, C. C. Chang, and E. Diener, Phys. Rev. Lett. **28**, 766

- (1972).
- <sup>20</sup>B. M. K. Nefkens, Th. S. Bauer, K. Baba, A. Boudard, W. J. Briscoe, G. Bruge, J. L. Faure, J. Gosset, A. Hegerath, J. S. Lugol, B. H. Silverman, and Y. Terrien, *Phys. Rev. Lett.* **45**, 168 (1980).
- <sup>21</sup>C. A. Heusch, R. V. Kline, K. T. McDonald, and C. Y. Prescott, *Phys. Rev. Lett.* **37**, 405 (1976); C. A. Heusch, R. V. Kline, K. T. McDonald, J. B. Carroll, D. H. Frederickson, M. Goitein, B. Macdonald, V. Perez-Mendez, and A. W. Stetz, *ibid.* **37**, 409 (1976).
- <sup>22</sup>P. E. Argan, G. Audit, N. deBotton, J.-L. Faure, J.-M. Laget, J. Martin, C. G. Schuhl, and G. Tamas, *Nucl. Phys.* **A237**, 447 (1975).
- <sup>23</sup>P. Picozza, C. Schaerf, R. Scrimaglio, G. Goggi, A. Piazzoli, and D. Scannicchio, *Nucl. Phys.* **A157**, 190 (1970).
- <sup>24</sup>J. Arends, J. Eyink, A. Hegerath, H. Hartmann, B. Meeking, G. Noldeke, and H. Rost, *Nucl. Phys.* **A322**, 253 (1979).
- <sup>25</sup>D. J. S. Findlay, R. O. Owens, M. J. Leitch, J. L. Matthews, C. A. Peridier, B. L. Roberts, and C. P. Sargent, *Phys. Lett.* **74B**, 305 (1978).
- <sup>26</sup>J. L. Matthews, W. Bertozzi, M. J. Leitch, C. A. Peridier, B. L. Roberts, C. P. Sargent, W. Turchinets, D. J. S. Findlay, and R. O. Owens, *Phys. Rev. Lett.* **38**, 8 (1977).
- <sup>27</sup>J. L. Matthews, in *Proceedings of the International Conference on Nuclear Physics with Electromagnetic Interactions, Mainz, 1979*, edited by H. Arenhovel and D. Drechsel (Springer, Berlin, 1979).
- <sup>28</sup>J. L. Matthews, D. J. Findlay, S. N. Gardiner, and R. O. Owens, *Phys. Lett.* **46B**, 186 (1973); *Nucl. Phys.* **A267**, 51 (1976).
- <sup>29</sup>D. J. S. Findlay, D. J. Gibson, R. O. Owens, and J. L. Matthews, *Phys. Lett.* **79B**, 356 (1978).
- <sup>30</sup>D. J. S. Findlay and R. O. Owens, *Phys. Rev. Lett.* **37**, 674 (1976); *Nucl. Phys.* **A279**, 385 (1977); *ibid.* **A292**, 53 (1977).
- <sup>31</sup>H. G. Miller, W. Buss, and J. A. Rawlins, *Nucl. Phys.* **A163**, 637 (1971).
- <sup>32</sup>H. Schier and B. Schoch, *Nucl. Phys.* **A229**, 93 (1974); *Lett. Nuovo Cimento* **12**, 334 (1975).
- <sup>33</sup>H. Hebach, M. Wortberg, and M. Gari, *Nucl. Phys.* **A267**, 425 (1976).
- <sup>34</sup>H. Hebach, in *Proceedings of the International School on Electro and Photonuclear Reactions, Erice, Italy, 1976*, edited by S. Costa and C. Schaerf (Springer, New York, 1977).
- <sup>35</sup>M. Gari and H. Hebach, *Phys. Rep.* **72**, 1 (1981).
- <sup>36</sup>J. T. Londergan, G. D. Nixon, and G. E. Walker, *Phys. Lett.* **65B**, 427 (1976).
- <sup>37</sup>J. T. Londergan and G. D. Nixon, *Phys. Rev. C* **19**, 998 (1979).
- <sup>38</sup>B. Schoch, *Phys. Rev. Lett.* **41**, 80 (1978).
- <sup>39</sup>M. A. Kovash, S. L. Blatt, R. N. Boyd, T. R. Donoghue, H. J. Hausman, and A. D. Bacher, *Phys. Rev. Lett.* **42**, 700 (1979).
- <sup>40</sup>S. L. Blatt, M. A. Kovash, H. J. Hausman, T. R. Donoghue, R. N. Boyd, A. D. Bacher, and C. C. Foster, in *Proceedings of the Topical Conference on Giant Multipole Resonances, Oak Ridge, Tennessee, 1979*, edited by F. Bertrand (Harwood, New York, 1980).
- <sup>41</sup>S. L. Blatt, Los Alamos Scientific Laboratory Report No. LA-8303-C, 1980.
- <sup>42</sup>S. L. Blatt, private communication.
- <sup>43</sup>S.-F. Tsai and J. T. Londergan, *Phys. Rev. Lett.* **43**, 576 (1979), referred to as TL.
- <sup>44</sup>M. Fink, H. Hebach, and K. Kummel, *Nucl. Phys.* **A186**, 353 (1972).
- <sup>45</sup>V. Gillet and N. Vinh Mau, *Nucl. Phys.* **54**, 321 (1964).
- <sup>46</sup>T. W. Donnelly and G. E. Walker, *Ann. Phys. (N.Y.)* **60**, 209 (1970).
- <sup>47</sup>A. J. F. Siegert, *Phys. Rev.* **52**, 787 (1937).
- <sup>48</sup>D. Halderson and R. J. Philpott, *Phys. Rev. Lett.* **46**, 100 (1981).
- <sup>49</sup>D. Halderson and R. J. Philpott (unpublished).
- <sup>50</sup>L. G. Arnold, *Phys. Rev. Lett.* **42**, 1253 (1979).
- <sup>51</sup>H. R. Weller, private communication.
- <sup>52</sup>I. Abdul-Jalil and D. F. Jackson, *J. Phys. G* **5**, 1699 (1979); D. F. Jackson and I. Abdul-Jalil, *ibid.* **6**, 481 (1980).
- <sup>53</sup>S. Boffi, C. Giusti, and F. D. Pacati, *Nucl. Phys.* **A359**, 91 (1981).
- <sup>54</sup>J. Mougey, M. Bernheim, A. Bussiere, A. Gillebert, Phan Xuan Ho, M. Priou, D. Royer, I. Sick, and G. T. Wagner, *Nucl. Phys.* **A262**, 461 (1976).
- <sup>55</sup>D. M. Brink and G. R. Satchler, *Angular Momentum* (Clarendon, Oxford, 1968).
- <sup>56</sup>A. Messiah, *Quantum Mechanics* (North-Holland, Amsterdam, 1961).